

ARTICLE OPEN



Skin-integrated, biocompatible, and stretchable silicon microneedle electrode for long-term EMG monitoring in motion scenario

Huawei Ji^{1,5}, Mingyu Wang^{1,5}, Yutong Wang², Zhouheng Wang², Yinji Ma², Lanlan Liu³, Honglei Zhou^{2,3}, Ze Xu¹, Xian Wang⁴, Ying Chen³✉ and Xue Feng²✉

Electromyography (EMG) signal is the electrical potential generated by contracting muscle cells. Long-term and accurate EMG monitoring is desirable for neuromuscular function assessment in clinical and the human–computer interfaces. Herein, we report a skin-integrated, biocompatible, and stretchable silicon microneedle electrode (SSME) inspired by the plant thorns. The silicon microneedles are half encapsulated by the polyimide (PI) to enhance the adaptability to deformation and resistance to fatigue. Thorn-like SSME is realized by the semi-additive method with a stretchability of not less than 36%. The biocompatibility of SSME has been verified using cytotoxicity tests. EMG monitoring in motion and long-term has been conducted to demonstrate the feasibility and performance of the SSME, which is compared with a commercial wet electrode. Hopefully, the strategies reported here can lead to accurate and long-term EMG monitoring, facilitating an effective and reliable human–computer interface.

npj Flexible Electronics (2023)7:46; <https://doi.org/10.1038/s41528-023-00279-8>

INTRODUCTION

To comprehensively and thoroughly merge the biological world into information networks requires all types of interfaces that can translate the bio-signal to an electric signal with high safety and accuracy. A wearable soft platform featuring dry needle electrodes and shielded stretchable interconnects was used for visual potential decoding¹. Epidermal electronics have been proposed to act as an interface². More than 20 years have witnessed the development of materials, structures, and fabrication methods for many skin-like/bioelectronic devices, and their applications, ranging from continuous physiological/biochemical parameter collection to drug delivery^{3–9}. Electromyography (EMG) signals, as the electric potential in the muscle cells, are an intuitive interface for human–computer interaction (HCI), particularly the surface EMG^{10–13}.

The difficulty of EMG detection is mainly caused by the high impedance of the skin's stratum corneum and motion artifacts¹⁴. The conventional surface myoelectric electrode is an Ag/AgCl wet electrode. The conductive gel is introduced to stick the Ag/AgCl wet electrodes onto the human skin, containing a certain amount of conductive ions, to significantly reduce the electrode–skin contact resistance. However, the skin of users should be cleaned with exfoliation, which may lead to allergic reactions^{15,16} and increase the psychological burden on the subject^{17,18}. Furthermore, the conductive paste of wet electrodes dries up over time, causing a significant increase in the skin-electrode contact impedance and performance degeneration^{18,19}.

To handle the long-term monitoring applications, dry electrodes have been proposed but it is suffer from high impedance due to the stratum corneum^{20,21}. The stratum corneum is mainly composed of corneocytes, which are dead cells without nuclei embedded into the highly ordered and dense lipid matrix. The moisture content of the Stratum Corneum is maintained at about

20%. It is believed that such a structure and composition determine the hydrophobic properties of the skin and narrow transport channel, which has a high skin impedance²². Thus, microneedle structures are introduced into the dry electrode. The microneedle electrode can penetrate into the stratum corneum, greatly reducing contact impedance and maintaining stable impedance over time for long-term detection^{23,24}. Different materials and fabrication methods have been proposed to realize desirable microneedle electrodes^{25,26}. A microneedle sensor was developed using a hybrid substrate based on high-Young's modulus epoxy siloxane for the microneedles and low-Young's modulus polydimethylsiloxane for the conformable substrate²⁷. Krieger et al. developed a stainless-steel microneedle electrode using the direct metal laser sintering (DMLS) 3D printing process, and the device could record surface EMG signals for up to 6 h with a signal-to-noise ratio comparable to that of wet electrodes²⁸. A microneedle electrode array composed of stainless-steel microneedles and polydimethylsiloxane (PDMS) substrate allows for large-area monitoring, and the wires can withstand up to 63% tensile strain²⁹. However, impedance changes within a certain range when the device is stretched. The bent substrate can be used to compensate for the curvature of the skin and maintain stable contact during measurements³⁰. However, the curvature is fixed and cannot dynamically adapt to the morphology of the skin. A microneedle electrode made of polyimide (PI) by molding, integrated with a flexible printed circuit board (PCB), enables the recording and wireless transmission of high-density surface electromyography signals³¹.

Silicon has good modifiability, chemical stability, and high hardness, and it is the core material used in the semiconductor industry with systematically mature processing methods. A silicon microneedle electrode containing through-holes was fabricated by the double-sided KOH bulk etching technique, such that the

¹School of Mechanical Engineering, Hangzhou Dianzi University, 310018 Hangzhou, China. ²AML, Department of Engineering Mechanics, Center for Flexible Electronics Technology, Tsinghua University, 100084 Beijing, China. ³Institute of Flexible Electronics Technology of THU, 314000 Jiaxing, Zhejiang, China. ⁴Qiantang Science and Technology Innovation Center, 310018 Hangzhou, China. ⁵These authors contributed equally: Huawei Ji, Mingyu Wang. ✉email: chenying@ifet-tsinghua.org; fengxue@tsinghua.edu.cn

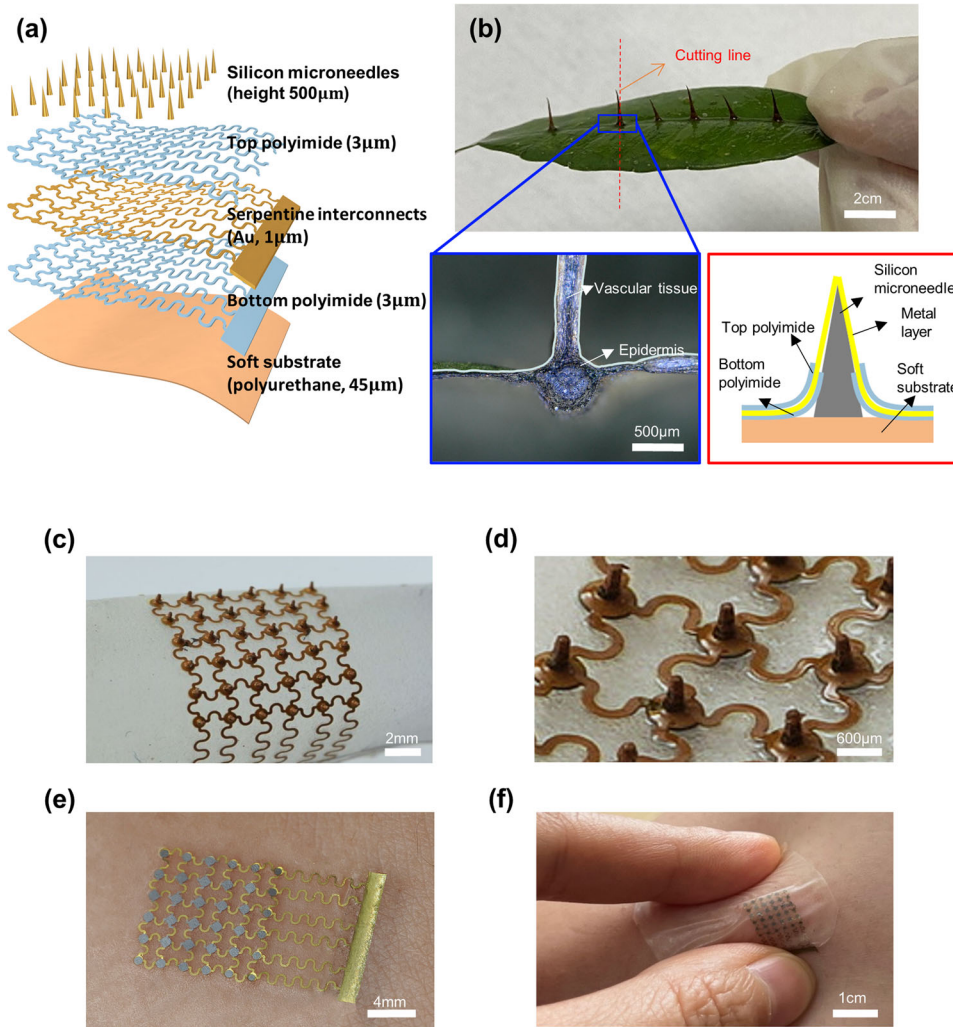


Fig. 1 Design of the SSME. **a** Exploded view of the SSME; **b** Thorns on the leaf surface of a *Radix Zanthoxyli* with a cross-sectional view of the thorn and bioinspired structure of the SSME; **c** SSME wrapped on a glass rod; **d** Detailed view of the silicon microneedles and serpentine interconnects; **e** SSME is attached to the skin; **f** SSME on the skin undergoes pinching.

front-to-back electrical contact was established for the convenience of signal transmission²⁴. Wang prepared a flexible microneedle electrode array by a KOH-scoring-KOH etching process based on silica-glass bonded sheets and realized the competitive impedance density of $7.5 \text{ k}\Omega\text{-cm}^2@10 \text{ Hz}$ ³². However, these silicon-based microneedles are neither stretchable enough to accommodate the movement and deformation of the skin and muscle, nor sufficiently robust to relieve concerns regarding the rupture of the microneedles during the collection of signals in the muscle.

In this paper, we report a strategy for designing and fabricating a skin-integrated, biocompatible, robust, and stretchable silicon microneedle electrode (SSME) for long-term EMG monitoring in a motion scenario. The structure of SSME is inspired by the thorns of plants, which are usually wrapped within a layer of the epidermis, particularly at the thorn's root, to keep them firmly standing on leaves or stems. The SSME consisted of silicon microneedles, serpentine interconnects encapsulated with PI, and a polyurethane substrate. The roots of the microneedles were buried within the sandwiched layers of the bottom PI/metal/top PI. The plant thorn-like structure increases the contact area between the microneedles and flexible substrate, enhancing the interfacial strength, and mitigates the stress concentration at the root of the microneedles undergoing deformation. This structure, together

with the serpentine interconnects, is obtained by a semi-additive process. Tensile and fatigue tests have been performed to verify the reliability of SSME. The safety of the device is verified by cytotoxicity tests, and the results show that the device is biocompatible and safe to wear for a long time. Impedance tests and surface electromyography measurements are performed on the subject's muscle tissue, in contrast to conventional wet electrodes. Furthermore, surface EMG signals are measured for both electrodes at 0 and 6 h during exercise. The results show that SSME has a comparable surface EMG recording ability to wet electrodes and better results in long-term motion scenes. These features highlight the promising potential of SSME for wearable healthcare monitoring, myoelectric prostheses, and human-computer interfaces.

RESULTS

Design and preparation of SSME

As shown in Fig. 1a, the SSME consists of silicon microneedles, serpentine interconnects enveloped by PI, and a polyurethane substrate. Silicon microneedles with a relatively large Young's modulus pierce through the stratum corneum easily, compared with other materials such as SU-8 or PDMS. Gold is adopted as the conductive layer in the electrode and interconnects owing to its

good biocompatibility and resistance to oxidization and corrosion. The interconnects are shaped into a serpentine style and encapsulated with PI to ensure stretchability. A semipermeable polyurethane film (Opsite, Smith & Nephew) with an adhesive layer (polyvinyl ethyl ether) is used as the soft substrate. The thickness of the soft substrate is only 45 μm , and Young's modulus is 4.68 MPa while that of the skin is 4.6–20 MPa³³. Thus, the SSME's materials and structural design ensure that the device's attachment to the human skin is seamless and painless.

Material and structural interface design is essential to improve interface adhesion and prevent damage to electromechanical properties under mechanical deformation³⁴. The detailed structure of the microneedles is learnt from the plant thorn structures of *Radix Zanthoxyli*, as shown in Fig. 1b. As shown in the microscopic image of the longitudinal dissection of the thorns, the structure of the thorns mainly consists of the fibrovascular tissue of the thorns and the surface layer of the epidermis wrapping over them, which makes them resistant to detachment, tilting, or rupture. Inspired by this, the surface of the microneedle is partially covered by two layers of PI like the epidermis. It increases the contact area between the microneedles and flexible substrate and enhances the interface strength, while the tip is left out to receive and transmit the electrical signals.

The final product of SSME is pliant and ready for integration on curved surfaces. Figure 1c shows SSME wrapped around a glass rod, demonstrating its flexibility. The details of the SSME in the flat state are shown in Fig. 1d, in which the silicon microneedles stand on the soft substrate, and their roots are surrounded by the PI/metal/PI sandwiched thin films. The height of the microneedle is 500 μm and the bottom diameter is 350 μm . The layout of the microneedles, particularly the space density, is such important that it influences both the signal-to-noise ratio (SNR) and shape of the fabricated microneedle forest. The smaller the space the larger the SNR, and the microneedle forest becomes shorter in the periphery yet higher in the middle with non-uniform shapes. The central interval between any two adjacent microneedles for the 6 \times 6 array is 1.2 mm.

Finite element analysis is used to evaluate the mechanical properties of the SSME. As shown in Supplementary Fig. 1, three finite element models of the traditional microneedle electrode, the proposed microneedle electrodes bonded with bionic structures with the thickness of 6 and 12 μm , respectively, are established. In the simulations, all the models are meshed by the 8-node liner brick element (C3D8R). A shear stress of 1 N is applied on the top surface of the microneedle with the soft substrate (PU) fixed at the bottom surface. Static, general analyses are completed to calculate the contact stress of the interface between the microneedle and soft substrate. The value of the maximum microneedle/PU substrate interface contact stress for the microneedle electrode bonded with a bionic structure (with a thickness of 6 μm) is about 45% smaller than that of the traditional microneedle electrode. Furthermore, the maximum interface contact stress has a 10% reduction with the thickness of the bionic structure (PI) increasing from 6 to 12 μm . The results show that the structure of SSME can resist detachment, tilt, and rupture.

When wearing the device, the silicon microneedles pierce the stratum corneum and are attached to the skin by the adhesive layer of the soft substrate, as shown in Fig. 1e. Owing to the stretchable design, the SSME can conform to the curved surface and dynamically accommodate skin deformation. Figure 1f shows the physical condition of the device with human skin undergoing pinching.

As shown in Fig. 2a, the fabrication of SSME starts with the preparation of silicon pillars by deep reactive ion etching (DRIE) with a depth of 500 μm . Then, the silicon pillars are isotropically etched by a mixed acid solution for 15–20 min to transform the pillars into microneedles. The mixed acid solution is HF: HNO₃: CH₃COOH = 3:25:10 in mass ratio, in which HNO₃ oxidizes Si to

SiO₂ on the surface of silicon, HF decomposes SiO₂ away, and CH₃COOH plays as a buffering role. Before spin-coating of PAA (polyamic acid, PAA-1002, China), the surface of the microneedles is treated with oxygen plasma for 5 min to ensure the adhesion of PAA. Thorough curing is conducted to make the chemical properties of the PI stable and not easily destroyed. The curing process is set to 80 °C for 20 min, 120 °C for 20 min, 150 °C for 30 min, 180 °C for 30 min, 200 °C for 10 min, 220 °C for 20 min, and 250 °C for 30 min. After curing the PAA into PI, the next step was to prepare the serpentine interconnects on the device with silicon microneedles. Here, we adopt the semi-additive method, the details of which are shown in Supplementary Fig. 2. It is started by sputtering a layer of titanium (Ti) with a thickness of 20 nm, and then a layer of gold (Au) with a thickness of 200 nm, in which titanium acts as the adhesive layer between the gold and the PI/silicon. A layer of photoresist (PR) is spin-coated on the device and patterned by lithography, in which the serpentine graph is left unprotected by the PR. The partially protected metal layer is then plated with 2 μm thick gold. After the PR is cleaned, the protected thin metal layer (with a thickness of 220 nm) is removed by wet etching, leaving thicker serpentine interconnects (with a thickness of 2 μm) as stretchable conductive layers in the device. The top PI film is then spin-coated, and both PI layers are patterned by reactive ion etching (RIE) with the copper layer as the hard mask. Finally, the fabrication is completed by removing its bottom silicon using RIE from the backside and transferring the device onto the soft PU substrate.

The morphology of the microneedles is examined using scanning electron microscopy (SEM) after wet etching, PI spin-coating, and metal sputtering, as shown in Fig. 2b–e, respectively. The profile of the silicon microneedle remains the same during all thin-film fabrication steps. The diameter of the tips is 10–50 μm , which is sufficient for piercing human tissues. More importantly, the PI layer covers the serpentine interconnects and extends halfway up the microneedles, as demonstrated by the distribution of carbon elements measured in the SEM shown in Fig. 2d. This mimickers the epidermis of the plant thorn while leaving the upper microneedles uninsulated to transmit the EMG signal.

Mechanical test

To test the stretchability and resistance to tensile deformation fatigue, the SSME has been stretched repeatedly using the setup shown in Fig. 2f, and the process is shown in Supplementary Video 1. Figure 2g, h show magnified views of the gold interconnects before and after 1000 cycles of stretching and relaxation within 20% elongation. No cracks, delamination, or wrinkle failures occur after repeated stretching, and the entire device is within the elastic deformation range because of the stretchable design. Meanwhile, it indicates the ability of SSME to accommodate random and dynamic deformations on the human body in motion scenes. Specifically, when the SSME is stretched, the deformation follows the classic “island-bridge” model in flexible and stretchable electronics³⁵. The serpentine interconnects bend and flip to accommodate the tensile stress passed on by the soft substrate as the “bridge,” while the silicon microneedles remain unchanged as the “island.” Figure 2i–l shows the interconnects and microneedles zoom-in pictures with no deformation and with a tensile strain of 24% and 36%, respectively. The S-shaped interconnects turns out of the plane to release the in-plane stress concentration, and the silicon microneedles stick to the substrate. The stretching and fatigue test results indicate that the SSME design and fabrication methods are valid in terms of being robust in handling the repeated and dynamic deformation of the human skin in motion.

To further demonstrate the stretchability of the device, we have stretched the device by the home-made loading stage while measuring its electric resistance. As is shown in Supplementary Fig. 3, the resistance does not change with the increase of

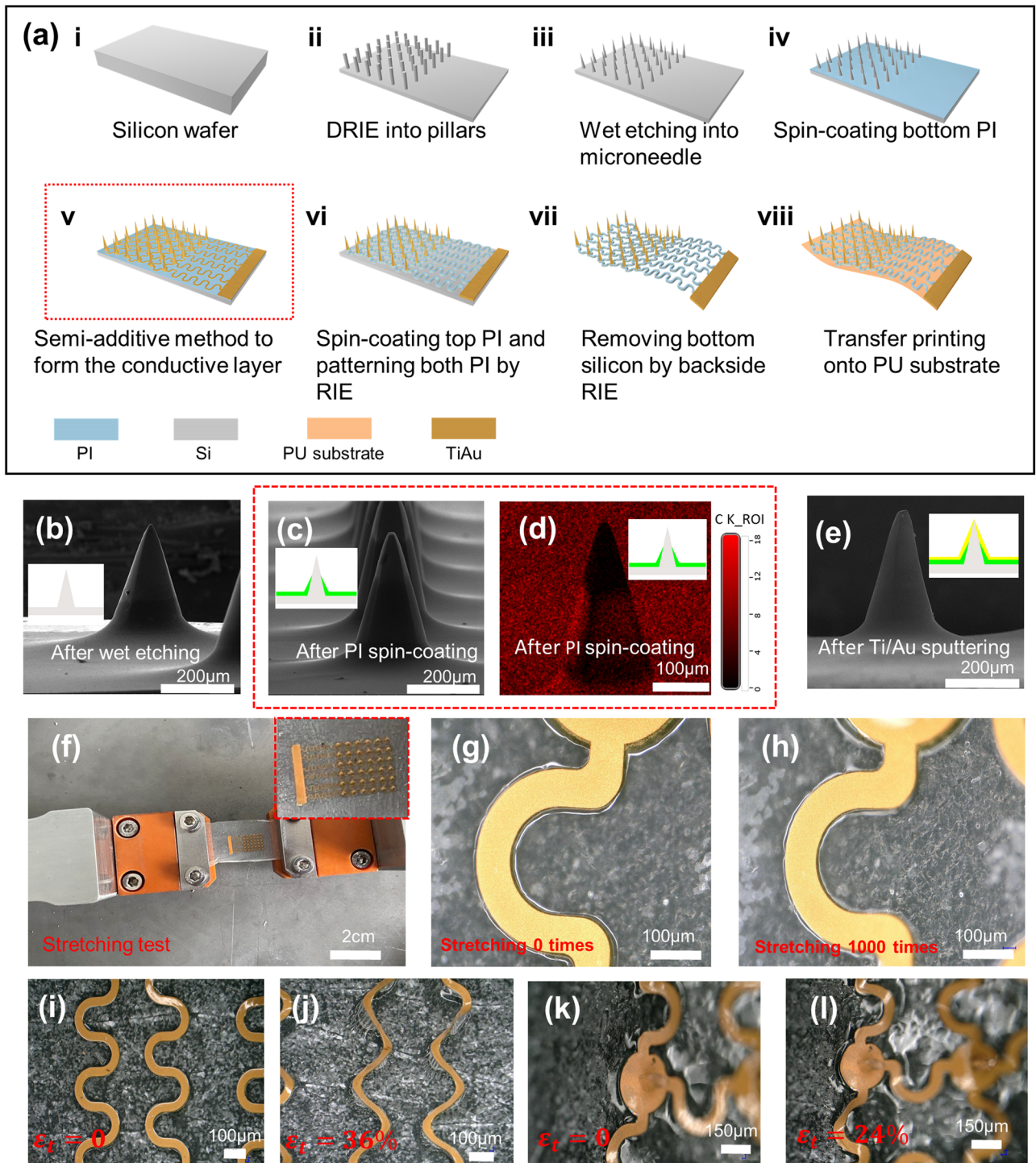


Fig. 2 Fabrication of the SSME. **a** Process flow for fabricating the SSME; **b** SEM image of silicon microneedle morphology after isotropic wet etching; **c** SEM image of silicon microneedle morphology after spin-coating PI; **d** Image of carbon elemental analysis in electron microscope after spin-coating PI; **e** SEM image of microneedle morphology after metal sputtering; **f** Setup for the stretching test; **g** Microscope image of serpentine interconnect for stretching zero times and **h** 1000 times; **i** Microscope image of serpentine interconnector before being stretched and **j** stretched at 36%; **k** Microscope image of microneedle before being stretched and **l** stretched at 24%.

stretching deformation. Results show that in the range of 45% stretching deformation, the SSME's resistance is stable with variation below 0.5%. Also, We applied 100 cyclic loadings of 24% strain to SSME using a tensile testing machine and measured the skin interface impedance of the electrodes before and after loading. The results are shown in Supplementary Fig. 4, it shows

that 100 stretches have a negligible effect on the impedance of SSME.

Electrical test

Electrode–skin contact impedance is an important indicator of the performance of physiological electrodes and has a direct impact

on the acquisition of physiological electrical signals. Electrode–skin contact impedance is generally tested using the double-electrode method. Here, an impedance analyzer is adopted to offer a constant small current from the positive input to the negative output to form a pathway. The contact impedance is then scanned at different frequency values. As the main frequency range of the myoelectric signal is usually between 0 and 500 Hz and the energy is concentrated around 50–150 Hz, the selected impedance scanning frequency range was 10–1000 Hz. Figure 3a shows the impedance scanning test results of both the SSME and wet electrode. It is shown that with an increase in the current frequency, the impedance of both gradually decreases. The impedance magnitude of the SSME is larger than that of the wet electrode at frequencies below 40 Hz, while it remains smaller in the range of 40–1000 Hz. The overall impedance amplitudes of the wet electrode and SSME are similar, indicating that the impedance performance of the SSME reached the level of the wet electrode.

The variation in the device's contact impedance with time is critical for long-term EMG monitoring. Impedance comparisons are made between 0 and 6 h for both the SSME and wet electrode. The impedance of the wet electrode is commonly recognized as unstable in the long-term because its conductivity is highly affected by both the environment and perspiration of the skin³⁶. High environmental temperature and low humidity expedite the gel drying and increase the impedance. Intense sweating enriches the conductive gel with water and conductive ions, resulting in a decrease in the impedance. However, the impedance of SSME is relatively immune to the environment and skin surficial perspiration, as it is pierced into the skin, enabling the electrical signal to be directly transmitted from the body. Figure 3b shows the SSME impedance at 0 and 6 h. The inset shows that the impedance of the SSME remains approximately 40–140 k Ω , and the impedance slightly decreases after 6 h of wearing. Contrarily, the impedance of the wet electrode is also measured at different times, as shown in Supplementary Fig. 5, together with its setup. The impedance variation rates of both the SSME and wet electrode are shown in Fig. 3c. The contact impedance of the SSME remains stable after 6-hour's of wearing in the large frequency range, whereas that of the wet electrode increases significantly, particularly in the low-frequency range. The above test results prove that the SSME has a more stable impedance performance than the wet electrode, which is more suitable for long-term EMG signal monitoring.

Simulation of the piercing process

The SSME is a minimally invasive device used for wearable EMG monitoring. However, to further demonstrate the safety of long-term wearing of the SSME, the penetration study is conducted on human skin tissues. Numerical simulation based on finite element analysis has been conducted to study the process of the insertion of micro-needles into the human skin^{37,38}. As a result, the skin deformation and the stress distribution on it, as well as the corresponding insertion force were obtained³⁹. According to previous studies, the failure strength of human skin is approximately 37 MPa, and therefore we can estimate the required force to pierce the micro-needle into the skin is 0.1387 N as shown in Supplementary Fig. 6. While wearing the SSME, the silicon microneedles are pierced into the skin. As shown in the left picture of Fig. 3d, the clear imprints resembling the size and layout of the silicon microneedles indicate that SSME can easily penetrate the stratum corneum. After 30 min, the array of fine pores on the skin diminishes to some degree. Two hours later, the skin fully involuntarily recovers without any redness or imprinting, as shown in Fig. 3d. No other abnormalities were found on the skin in the subsequent 48 h, which verified the SSME's safety.

Biocompatibility test

However, SSME is biocompatible and resistive to the subsurface bio-environment of human skin during long-term wearing. Thus, PBS buffer is used to simulate the human interstitial fluid, and SSME is placed in PBS buffer for 72 h. Morphological characterization and elemental analysis of the electrode surfaces performed by the SEM before and after PBS buffer immersion are shown in Fig. 3e, h, respectively. Clearly, the morphology of the microneedle remains almost the same as the original state, with no corrosion or crack signs. The elemental distribution on the surface of the electrodes soaked in PBS buffer for a long time is unchanged, indicating that the electrodes are not corroded in the tissue fluid. These results prove that SSME can be well adapted to the human tissue environment, which guarantees that the electrode can work properly in the human body for a long time.

Moreover, microneedle-like minimally invasive devices should avoid causing adverse effects on human tissues or organs⁴⁰. As SSME is in direct contact with human tissues during operation, it is necessary to verify the biocompatibility of the prepared electrodes in terms of cytotoxicity. The entire SSME device, silicon microneedles without PU soft substrate (with only PI/metal/PI sandwiched interconnects), and bare silicon are placed into the cultured human keratin-forming cells (HacaT) as the experimental groups, while the control group had nothing. The experimental and control groups are cultured under the same conditions. The HacaT cell viability assay (CCK8) and cell fluorescence staining (Calcein AM/PI) are used to estimate the effects of SSME on cells. Fig. 3i–k shows the staining results of the cells cultured by the entire SSME device for 24, 48, and 72 h, respectively. Fig. 3l shows the staining results of the cells cultured for 72 h in the blank control group. Green dots represent live cells and red dots represent dead cells. Clearly from the results, the number of live cells in both the experimental and control groups increases significantly as time elapses, while the number of dead cells in both groups is similar and extremely low. Fig. 3m shows the cell viability of the four groups at 24, 48, and 72 h. The cell viability of the three experimental groups is at least 95% of that of the control group, satisfying the required 70% cell viability, as recommended by ISO 10993-5⁴¹. The p-values of the calculated statistics are greater than 0.05. It can be concluded that the effect of adding SSME entirely or partially as microneedles on cell activity is not significantly different compared to the control group. In addition to the above experimental data, the systematic cell staining results of the experimental and control groups are shown in Supplementary Figs. 7–10. The above experimental results prove that SSME has good biosafety and can be used on the human body for a long time.

Acquisition and analysis of EMG signal

The circuit consists of three core parts, including the main control module (No.1), signal conditioning module (No.2), and the power management module (No.3), as shown in Supplementary Fig. 11. The main control module has a Bluetooth SoC chip (DA14580) with microcontroller unit integrated inside, 16-bit analog-to-digital converter (ADS1118) and a flash chip (W25X20CLSNIG). The signal conditioning module consists of an Analog front-end chip (AD8232) for weak myoelectric signal extracting, amplifying, and filtering. The power management module is for lithium battery charging management. The main chip is ME4057, which is small in size and has a large charging current. It also has functions such as charging protection. No.4 is the interface for the electrode.

The EMG of the forearm flexor during fist clenching is monitored by wearing the SSME as the working electrode with a wet electrode as the reference. The working electrodes are placed along the muscle tissue, and the reference electrode is placed at a distant tissue unrelated to the measured tissue, as shown in Fig. 4a. The signal is extracted through the electrodes to the circuit

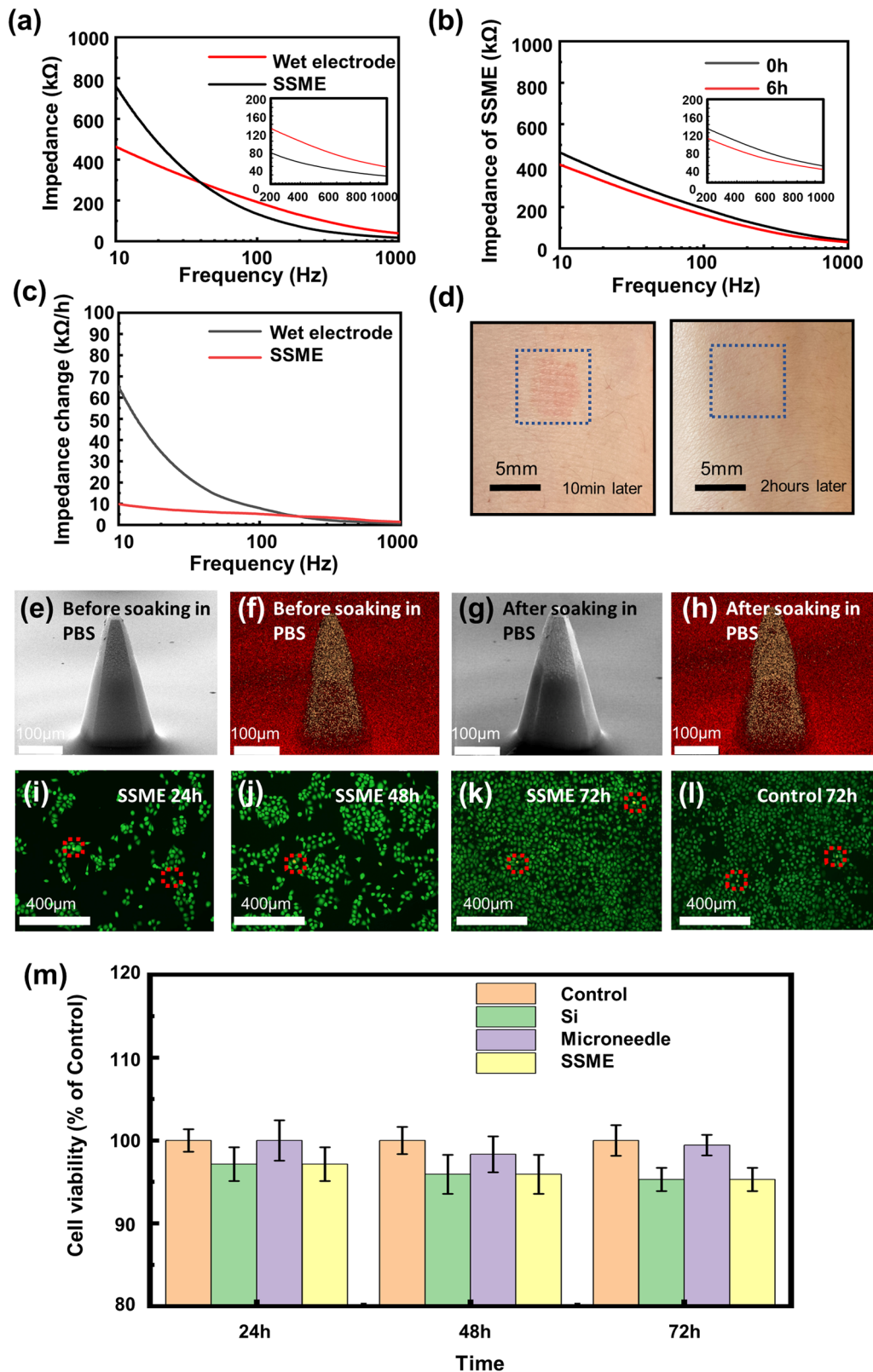


Fig. 3 Impedance tests and cytotoxicity experiments. **a** Impedance magnitude against frequency for the SSME with contrast to the wet electrodes; **b** Contact impedance of the SSME at 0 and 6 h; **c** Impedance change after 6 h for both the SSME and wet electrode; **d** Skin tissue after removing the SSME 10 min and 2 h; **e** SEM image and **f** Elemental distribution (Carbon in red, gold in yellow) of the SSME soaked in PBS solution at 0 h; **g** SEM image and **h** Elemental distribution (Carbon in red, gold in yellow) of the SSME soaked in PBS solution at 72 h; **i** Cell staining pictures of the experimental group at 24 h, **j** 48 h, **k** 72 h; **l** Cell staining pictures of the control group at 72 h; **m** Cell viability in the experimental with Si, microneedle, and entire SSME device and the control group.

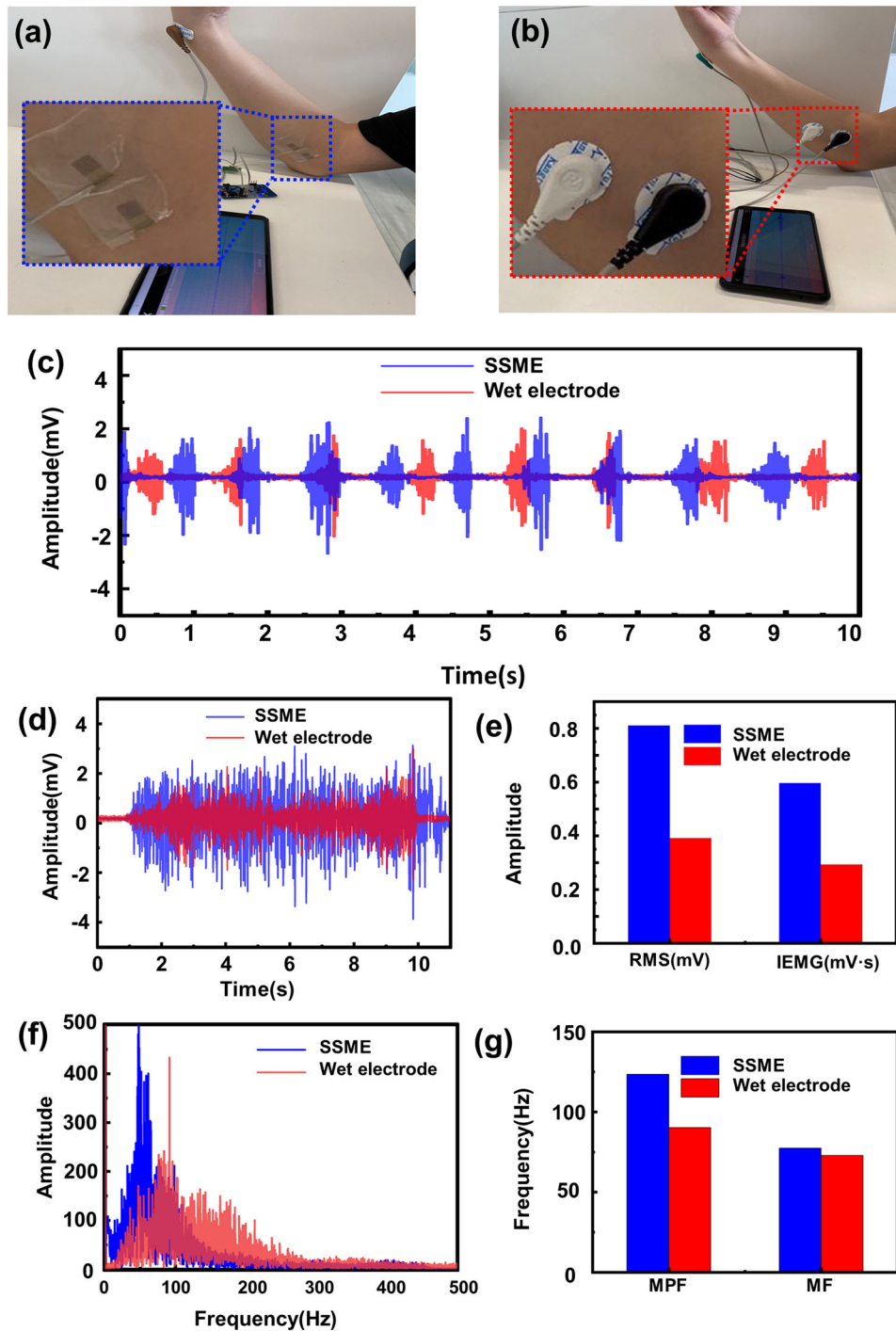


Fig. 4 Detection and analysis of EMG signal measured by the SSME. **a** Monitoring the EMG of the forearm flexor during fist clenching by wearing the SSME and **b** wet electrode; **c** EMG signal measured by the SSME and wet electrode during fist clenching; **d** Time domain of EMG signals measured by the SSME and wet electrode during continuous fist clenching; **e** Time-domain characteristics of EMG signals measured by the SSME and wet electrodes; **f** Frequency domain of EMG signals measured by the SSME and wet electrode during continuous fist clenching; **g** Frequency-domain characteristics of EMG signals measured by the SSME and wet electrodes.

board and then transmitted wirelessly using Bluetooth to the cell phone application to display the EMG signal in real-time. For comparison, wet electrodes are used to measure the same EMG signal, as shown in Fig. 4b. The experimental actions are set up as intermittent fist clenching and sustaining fist clenching. The EMG signal during intermittent fist clenching is shown in Fig. 4c. The measured EMG signal resembles the rhythm and duration of the clenching behavior. The EMG signal measured by the SSME is

similar to that collected by the wet electrode, and the amplitude of the former is relatively higher. The EMG signal of the sustaining fist clenching in the time domain is shown in Fig. 4d. The signal measured by the SSME is denser and of higher amplitude, indicating that the SSME has a higher signal extraction quality and signal-to-noise ratio than the wet electrode. More specifically, feature extraction in the time and frequency domains is conducted for the signals to sustain clenching. The root mean

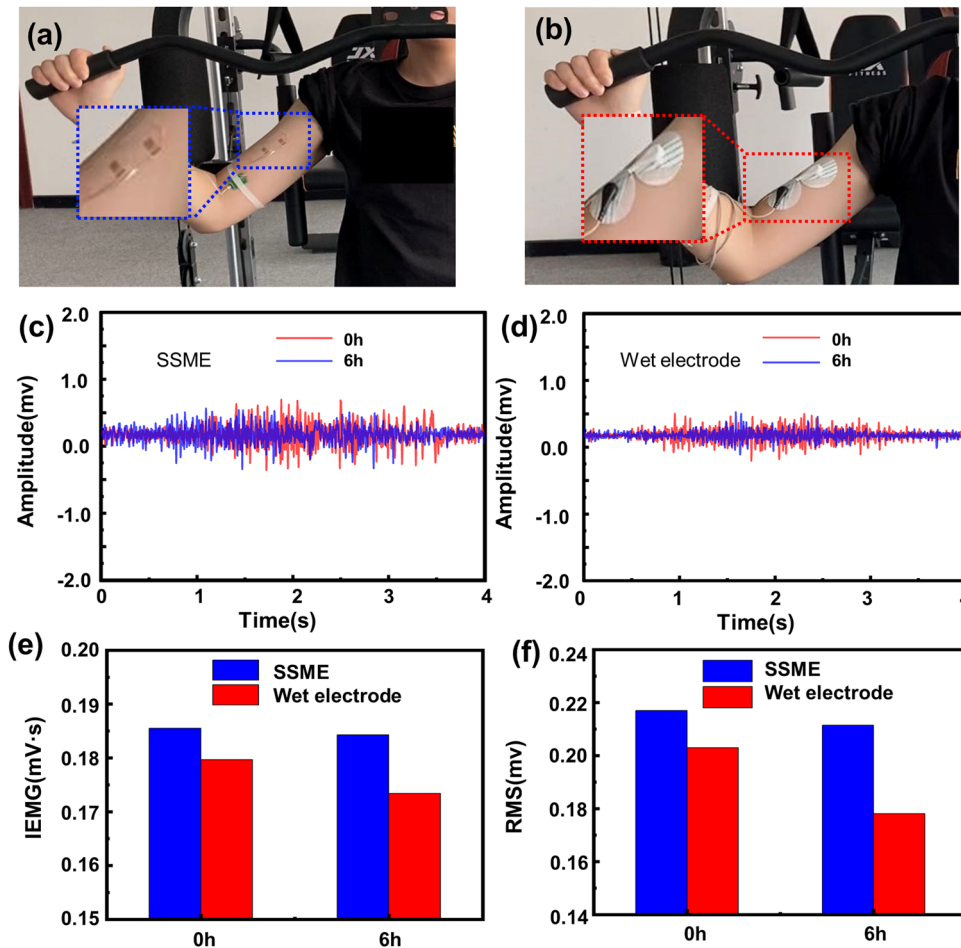


Fig. 5 Long-term monitoring of EMG signals in motion. **a** Monitoring the EMG of Biceps brachii muscle by wearing the SSME and **b** the wet electrode during high pull-down training; **c** EMG signals detected by the SSME and **d** the wet electrode at 0 and 6 h; **e** IEMG and **f** RMS of EMG signals measured at 0 and 6 h by the SSME and wet electrode.

square (RMS) value and integrated electromyographic (IEMG) value are two commonly used in time-domain feature metrics. RMS typically reflects the effective value of EMG, whereas IEMG reflects the activity state of the muscle. Figure 4e shows the RMS and IEMG values for both signals. Clearly, both the RMS and IEMG of SSME are higher than those of the wet electrode, which led to the conclusion that the quality of the EMG signal measured by the SSME is significantly higher than that of the wet electrode. This is because the microneedle penetrates the stratum corneum during the measurement process, which significantly reduces the electrode–skin contact impedance. However, the stretchability of SSME enables its adaptation to the deformation and motion of the skin, which greatly reduces motion artifacts. Further, the spectral analysis of EMG signals is performed by converting the time-domain signals into frequency-domain signals through Fourier transformation. Much information on the neuromuscular state of the motor unit can be obtained by analyzing the frequency information of the EMG signal⁴². From Fig. 4f, it can be observed that the EMG signal amplitudes of both the microneedle and wet electrodes are mainly concentrated in the range of 20–150 Hz; however, the signal amplitudes of the microneedle electrodes are higher. Figure 4g shows the mean power frequency (MPF) and median frequency (MF) of the two signals. This shows that the maximum power and median frequency values of the two signals were concentrated at different locations. If more frequency information is desired, it can be calculated using mathematical formulas^{43,44}.

To demonstrate the long-term detection of EMG signals during motion, measurements over prolonged periods in an exercise scenario are conducted. EMG signals of the biceps muscle are measured during muscle training using a high pull-down machine commonly used in gyms. The devices are continuously integrated into the human skin for 6 h. Signals are measured at 0 and 6 h. As shown in Fig. 5a, b, the electrodes are placed parallel to the biceps, and the rest of the experimental steps are the same as mentioned above. Generally, the amplitude of the SSME-measured signal is larger than that of the wet electrode. Moreover, the EMG signal measured by the SSME at 6 h is comparable to the result at 0 h (Fig. 5c), yet the EMG signal measured by the wet electrode at 6 h is somewhat lower than that at 0 h (Fig. 5d). Figure 5e, f show the time-domain characteristic values of the signals measured at 0 and 6 h for the two electrodes, respectively. Clearly, the IEMG and RMS of the SSME are larger than those of the wet electrode at 0 and 6 h. The decline of the IEMG and RMS of the SSME is much smaller than that of the wet electrode after 6 h, which shows the different performances of the SSME and wet electrode for continuous EMG monitoring. Long-time wearing and real-time monitoring results demonstrate that the SSME possesses a higher stable performance and comfortable wearing feature, which is more suitable for the continuous detection of EMG signals.

DISCUSSION

In this study, a stretchable silicon microneedle electrode has been proposed by imitating the structure of the thorn of radix

zanthoxyli. An array of silicon microneedles with a height of 500 μm is prepared by isotropic and anisotropic corrosion of silicon. Using the semi-additive method, a serpentine interconnector is fabricated on the microneedle, enabling a stretching rate of over 45%. With fixed piercing locations on the skin and stretchability, high-quality signal extraction can be ensured to decrease interference from skin deformation during daily movement, owing to the good compliance of the device to the skin. Cell experiments have demonstrated that SSME has good biocompatibility. Through impedance performance comparison, the SSME is verified to exhibit better stability than commercial wet electrodes, which can maintain a small change in impedance for a long time and be adapted to long-time and multiple scenes of EMG signal detection.

Nevertheless, further improvements are necessary to address challenges such as the high density of the microneedle electrode that can monitor the EMG signals with higher spatial resolution, as well as integrating the signal process IC chips into the flexible substrate to convert the analog signal into digital signal diminishing the transmission interference. Besides, application research of the skin-integrated microneedle electrode for the diagnosis or treatment of different diseases is worth doing. Hopefully, these skin-like EMG electrodes can revolutionize long-term EMG monitoring, enhancing our understanding and leading to more accurate diagnosis, personalized treatment, and improved patient outcomes.

METHODS

Fabrication of the flexible microneedle electrode

The process starts with preparing double-sided polished wafers (700 μm , P100) and cleaning the surface of the wafers. The microcolumn array on the wafer with a height of about 500 μm is formed by deep reactive ion etching (DRIE), and then etch them into microneedles in solution (HF: HNO_3 : CH_3COOH = 3:25:10) in a static state for about 10 min. The PAA (20% concentration) as the first flexible substrate layer is spinning-coated and thermally cured. Next, the conducting layer is prepared by sputtering with Ti(20 nm) and Au(200 nm) and masked by laser direct writing lithography. The unprotected gold layer is then thickened by electroplating to a thickness of about 2 μm , and the photoresist and excess Ti/Au are removed to complete the preparation of the serpentine wire. The second PI layer is prepared by spin-coating PAA (10% concentration) and curing. Sputtering Cu(200 nm) is acting as the mask layer to etch PI. The same laser direct writing and development is performed. The samples are placed in an RIE (O_2 , 90 W) to etch the PI and then the unwanted metal is removed. The final step is to remove the rigid substrate and transfer the device to the PU film, when microneedles are protected with PDMS and all the silicon on the backside is etched away using RIE (SF_6 , 120 W).

Numerical simulation

The finite element simulation software ABAQUS was used to evaluate the stability of the SSME structure when subjected to tangential forces. Three finite element models of conventional microneedle electrodes and the proposed microneedle electrodes bonded with bionic structures (PI with thicknesses of 0, 6, and 12 μm , respectively) were established. The models were meshed by 8-node linear brick, reduced integration, and hourglass control elements (C3D8R) with a global element size of 0.03 mm. The materials of the three layers of the whole microneedle structure from bottom to top are PU, PI, and Si, respectively. The height of the microneedle is 500 μm , the diameter of the bottom is 350 μm , and the thickness of the PU is 2 mm. The mechanical properties of the materials are $E_{\text{PI}} = 3.2$ GPa, $\mu_{\text{PI}} = 0.42$, $E_{\text{Si}} = 190$ GPa, $\mu_{\text{Si}} = 0.28$; and $E_{\text{PU}} = 0.69$ GPa, $\mu_{\text{PU}} = 0.3$. In the simulation, a 1 N shear force

was applied to the top of the microneedle, and the bottom surface of the PU layer was fixed. Through the static general analysis, the contact stresses at the interface between the microneedle and the soft substrate were obtained. Furthermore, the interaction between the micro-needle and skin during the process of the insertion of micro-needle into human skin was also simulated. In the finite element analysis, two-dimensional axisymmetric models for micro-needle and human skin were established to reduce the computational time. The micro-needle was modeled as an analytic rigid body because of its much greater stiffness than human skin. Furthermore, the incompressible hyperelastic Neo-Hookean Constitutive Model with the coefficient of $C10 = 10$ MPa and a density of 1300 kg/m³ was applied to human skin. The size of the microneedle is the same as described above, and the skin was established as a rectangular shell with a size of 5 \times 1 mm. The finite element model of human skin was meshed by 4-node bilinear axisymmetric quadrilateral elements (CAX4R) with the global element size of 0.05 mm, and the area in contact with the microneedle was meshed by refined elements with the smallest element size of 2 μm . Explicit dynamic analysis by applying displacement load to the microneedle was conducted to simulate the process of microneedle penetration into the skin with the sliding friction coefficient of 0.42 between the microneedle and human skin.

Ethical consideration

The experiments involving human subjects were performed with the full consent of the volunteers. All participants provided written informed consent.

DATA AVAILABILITY

The data that support the findings of this study are available from the corresponding author upon reasonable request.

Received: 28 March 2023; Accepted: 29 September 2023;
Published online: 17 October 2023

REFERENCES

- Mahmood, M. et al. VR-enabled portable brain-computer interfaces via wireless soft bioelectronics. *Biosens. Bioelectron.* **210**, 114333 (2022).
- Kim, D.-H. et al. Epidermal electronics. *Science* **333**, 838–843 (2011).
- Chen, Y. et al. Flexible inorganic bioelectronics. *NPJ Flex. Electron.* **4**, 1–20 (2020).
- Lee, H. et al. A graphene-based electrochemical device with thermoresponsive microneedles for diabetes monitoring and therapy. *Nat. Nanotechnol.* **11**, 566–572 (2016).
- Yu, J., Zhang, K. & Deng, Y. Recent progress in pressure and temperature tactile sensors: principle, classification, integration and outlook. *Soft Sci.* **1**, 6 (2021).
- Wong, T. H. et al. Tattoo-like epidermal electronics as skin sensors for human-machine interfaces. *Soft Sci.* **1**, 10 (2021).
- Du, Q. et al. High-performance flexible pressure sensor based on controllable hierarchical microstructures by laser scribing for wearable electronics. *Adv. Mater. Technol.* **6**, 2100122 (2021).
- Chen, Y., Lu, B., Chen, Y. & Feng, X. Breathable and stretchable temperature sensors inspired by skin. *Sci. Rep.* **5**, 1–11 (2015).
- Zhao, W., Liu, L., Lan, X., Leng, J. & Liu, Y. Thermomechanical constitutive models of shape memory polymers and their composites. *Appl. Mech. Rev.* **75**, 020802 (2022).
- Ahsan, M. R., Ibrahimy, M. I. & Khalifa, O. O. EMG signal classification for human computer interaction: a review. *Eur. J. Sci. Res.* **33**, 480–501 (2009).
- Chi, Y. M., Jung, T.-P. & Cauwenberghs, G. Dry-contact and noncontact biopotential electrodes: Methodological review. *IEEE Rev. Biomed. Eng.* **3**, 106–119 (2010).
- Ren, L., Liu, B., Zhou, W. & Jiang, L. A mini review of microneedle array electrode for bio-signal recording: a review. *IEEE Sens. J.* **20**, 577–590 (2019).
- Losey, D., McDonald, C., Battaglia, E. & O'Malley, M. K. A review of intent detection, arbitration, and communication aspects of shared control for physical human-robot interaction. *Appl. Mech. Rev.* **70**, 010804 (2018).

14. Farina, D., Merletti, R. & Enoka, R. M. The extraction of neural strategies from the surface EMG. *J. Appl. Physiol.* **96**, 1486–1495 (2004).
15. Avenel-Audran, M., Goossens, A., Zimerson, E. & Bruze, M. Contact dermatitis from electrocardiograph-monitoring electrodes: role of p-tert-butylphenol-formaldehyde resin. *Contact Derm.* **48**, 108–111 (2003).
16. Jelen, G. Acrylate, a hidden allergen of electrocardiogram electrodes. *Contact Derm.* **45**, 315–316 (2001).
17. Merletti, R. The electrode–skin interface and optimal detection of bioelectric signals. *Physiol. Meas.* **31**, E01 (2010).
18. Searle, A. & Kirkup, L. A direct comparison of wet, dry and insulating bioelectric recording electrodes. *Physiol. Meas.* **21**, 271 (2000).
19. Inoh, T. et al. Nanofiber web textile dry electrodes for long-term biopotential recording. *IEEE Trans. Biomed. Circuits Syst.* **7**, 204–211 (2013).
20. Lepola, P. et al. Screen-printed EEG electrode set for emergency use. *Sens. Actuators A Phys.* **213**, 19–26 (2014).
21. Baek, J. Y., An, J. H., Choi, J. M., Park, K. S. & Lee, S. H. J. S. Flexible polymeric dry electrodes for the long-term monitoring of ECG. *Sens. Actuators A Phys.* **143**, 423–429 (2008).
22. Lu, F. et al. Review of stratum corneum impedance measurement in non-invasive penetration application. *Biosensors* **8**, 31 (2018).
23. Srivastava, A. K., Bhartia, B., Mukhopadhyay, K. & Sharma, A. Long term biopotential recording by body conformable photolithography fabricated low cost polymeric microneedle arrays. *Sens. Actuators A Phys.* **236**, 164–172 (2015).
24. O'Mahony, C. et al. Microneedle-based electrodes with integrated through-silicon via for biopotential recording. *Sens. Actuators A Phys.* **186**, 130–136 (2012).
25. Ali, R. et al. Transdermal microneedles—a materials perspective. *AAPS PharmSciTech* **21**, 1–14 (2020).
26. Fu, Y., Zhao, J., Dong, Y. & Wang, X. Dry electrodes for human bioelectrical signal monitoring. *Sensors* **20**, 3651 (2020).
27. Lee, W. et al. Conformable microneedle pH sensors via the integration of two different siloxane polymers for mapping peripheral artery disease. *Sci. Adv.* **7**, eabi6290 (2021).
28. Krieger, K. J. et al. Development and Evaluation of 3D-Printed Dry Microneedle Electrodes for Surface Electromyography. *Adv. Mater. Technol.* **5**, 2000518 (2020).
29. Guvanasen, G. S. et al. A stretchable microneedle electrode array for stimulating and measuring intramuscular electromyographic activity. *IEEE Trans. Neural Syst. Rehabilitation Eng.* **25**, 1440–1452 (2016).
30. Kim, M., Kim, T., Kim, D. S. & Chung, W. K. Curved microneedle array-based sEMG electrode for robust long-term measurements and high selectivity. *Sensors* **15**, 16265–16280 (2015).
31. Wang, Z., Li, J., Yu, B., Huang, D. & Li, Z. in *2022 IEEE 35th International Conference on Micro Electro Mechanical Systems Conference (MEMS)*. 345–348 (IEEE, 2022).
32. Wang, R., Jiang, X., Wang, W. & Li, Z. A microneedle electrode array on flexible substrate for long-term EEG monitoring. *Sens. Actuators B-Chem.* **244**, 750–758 (2017).
33. Pawlaczyk, M., Lelonkiewicz, M. & Wieczorowski, M. Age-dependent biomechanical properties of the skin. *Postepy Dermatol. Allergol.* **30**, 302–306 (2013).
34. Gong, S., Yap, L. W., Zhu, B. & Cheng, W. Multiscale soft–hard interface design for flexible hybrid electronics. *Adv. Mater.* **32**, 1902278 (2020).
35. Li, R., Li, M., Su, Y., Song, J. & Ni, X. An analytical mechanics model for the island-bridge structure of stretchable electronics. *Soft Matter* **9**, 8476–8482 (2013).
36. Swanson, D. K. & Webster, J. G. *A Model for Skin-electrode Impedance*. 117–128 (Academic Press, 1974).
37. Xiangqing, K., Chengwei, W. U. & Ping, Z. Numerical simulation of the process of inserting micro-needles into skin. *Sci. Technol. Rev.* **27**, 43–48 (2009).
38. Gardner, T. N. & Briggs, G. A. D. Biomechanical measurements in microscopically thin stratum corneum using acoustics. *Ski. Res. Technol.* **7**, 254–261 (2010).
39. Elkhyat, A., Courderot-Masuyer, C., Gharbi, T. & Humbert, P. Influence of the hydrophobic and hydrophilic characteristics of sliding and slidersurfaces on friction coefficient: in vivo human skin friction comparison. *Ski. Res. Technol.* **10**, 215–221 (2010).
40. Wang, L. et al. Biomechanical study on implantable and interventional medical devices. *Acta Mech. Sin.* **37**, 21 (2021).
41. International Organization for Standardization (ISO). ISO 10993-5:2009: Biological Evaluation of Medical Devices-Part 5: Tests for in Vitro Cytotoxicity. Geneva, Switzerland: ISO; (2009).
42. Canal, M. R. Comparison of wavelet and short time Fourier transform methods in the analysis of EMG signals. *J. Med. Syst.* **34**, 91–94 (2010).
43. Auchincloss, C. C. & McLean, L. The reliability of surface EMG recorded from the pelvic floor muscles. *J. Neurosci. Methods* **182**, 85–96 (2009).
44. Yamaguchi, T., Mikami, S. & Okada, K. Validity of a newly developed ultra-miniature cordless EMG measurement system. *Oral. Surg. Oral. Med. Oral. Pathol. Oral. Radio.* **104**, e22–e27 (2007).

ACKNOWLEDGEMENTS

We appreciate the financial support from the National Natural Science Foundation of China (Grant No. U20A6001, 11902292), Zhejiang Province Key Research and Development Project (Grant No. 2021C01183, 2021C05007-4).

AUTHOR CONTRIBUTIONS

All authors contributed to the preparation of this manuscript. H.J. and M.W. contributed equally. H.W.J.: visualization, methodology, conceptualization, theoretical guidance, and design. M.Y.W.: methodology, conceptualization, writing, data curation, design, and preparation. Y.T.W.: data curation, design, and preparation. Z.H.W.: theoretical guidance. Y.J.M.: theoretical guidance. L.L.L.: process assistance. H.L.Z.: performance evaluation. Z.X.: process assistance. X.W.: theoretical guidance. Y.C.: project administration, visualization, methodology, conceptualization, writing. X.F.: visualization, methodology, funding acquisition, project administration, resources.

COMPETING INTERESTS

The authors declare no competing interests.

ADDITIONAL INFORMATION

Supplementary information The online version contains supplementary material available at <https://doi.org/10.1038/s41528-023-00279-8>.

Correspondence and requests for materials should be addressed to Ying Chen or Xue Feng.

Reprints and permission information is available at <http://www.nature.com/reprints>

Publisher's note Springer Nature remains neutral with regard to jurisdictional claims in published maps and institutional affiliations.



Open Access This article is licensed under a Creative Commons Attribution 4.0 International License, which permits use, sharing, adaptation, distribution and reproduction in any medium or format, as long as you give appropriate credit to the original author(s) and the source, provide a link to the Creative Commons license, and indicate if changes were made. The images or other third party material in this article are included in the article's Creative Commons license, unless indicated otherwise in a credit line to the material. If material is not included in the article's Creative Commons license and your intended use is not permitted by statutory regulation or exceeds the permitted use, you will need to obtain permission directly from the copyright holder. To view a copy of this license, visit <http://creativecommons.org/licenses/by/4.0/>.

© The Author(s) 2023